A novel cohesive zone modelling approach to represent mixed mode loading and bond line thickness effects

Brock Watson[a], Michael J. Worswick[a] and Duane S. Cronin[a]

[a]*Department of Mechanical and Mechatronics Engineering, University of Waterloo, Waterloo, Canada*

Accurate representation of the traction-separation response for mixed mode loading in a cohesive zone model (CZM) is critical to predicting the response of adhesive joints in a number of applications, including transportation and vehicle crashworthiness. Traditionally, the Mode I and Mode II responses are treated independently, with mixed mode response determined by relationships between the degree of mode mixity and separation, potentially leading to overprediction of the plateau traction and underprediction of the plateau length in mixed mode loading. This poor fit is due to the indirect relationship between mixity and traction and having minimal fitting options for separation-to-plateau and softening. To address this limitation, a mixed mode CZM approach is proposed, based on measured mixed-mode traction-separation results for a toughened epoxy adhesive. The effects of bond line thickness were considered, to examine the ability of the proposed approach to include additional effects (beyond mode mixity) that are known to affect the traction-separation response. The CZM implementation was assessed using the original test data and was shown to capture the measured experimental traction-separation response across a range of mixed mode loading and bond line thickness more accurately compared to traditional CZM treatments.

Keywords: cohesive zone modeling, mixed mode loading, bond line thickness, adhesive joining, finite element modeling

1 Introduction

While a number of approaches can be used to model the failure of adhesive joints [1], one of the most attractive methods to simulate adhesive joints in large-scale explicit finite element models is to represent the joint using a cohesive zone model (CZM) [2-4]. The CZM approach has bee used in analysis for fields as varied as dental implants [5], flexible piping structures for the oil sector [6], and bonding of dissimilar metals for advanced body-in-white design applications [37]. An interface or thin layer where a crack may initiate and propagate can be modeled using CZM elements, without the need for a predefined defect in the bond line [8], defined using a traction-separation response [9]. A general limitation of this method is that the path of the crack must be known prior to defining the model geometry; however, the crack path for modern structural adhesives with thin bond lines (on the order of 0.2 mm to 1 mm) can be approximated using the CZM method. Implementations of CZMs usually involve defining the Mode I and Mode II traction-separation response independently, which are often simplified to bi-linear [10] or trapezoidal [11,12] shapes for ease of implementation in finite element codes, while still representing adhesive joint responses. For modeling toughened adhesive joints the trapezoidal shape is often used [13-15]. A trapezoidal traction-separation curve (Figure 1) can be divided into three phases: the initial phase during which the traction is proportional to the separation, the plateau phase where the traction response is constant, and the softening phase, in which the traction reduces from the plateau value to zero. These regions are differentiated by the separation-to-plateau (δ^0) and separation-to-softening (δ^s) before failure occurs at the separation-to-failure (δ^f) value [4,16]. Fully defining a trapezoidal traction-separation response requires the initial slope of the traction-separation response (E), plateau traction (σ_0), critical energy release rate (G), and the ratio of area under the plateau to the area under the entire traction-separation response (termed area ratio (f), for brevity) to be defined. Trapezoidal CZM implementations commonly assume a constant plateau and do not allow for experimentally observed softening [17] or hardening [18]. Although some CZM implementations which include softening [17] and hardening [19] have been implemented in the literature, their adoption in popular finite element solvers has been limited. To account for the slope of the plateau, E_{Tan} must also be defined.

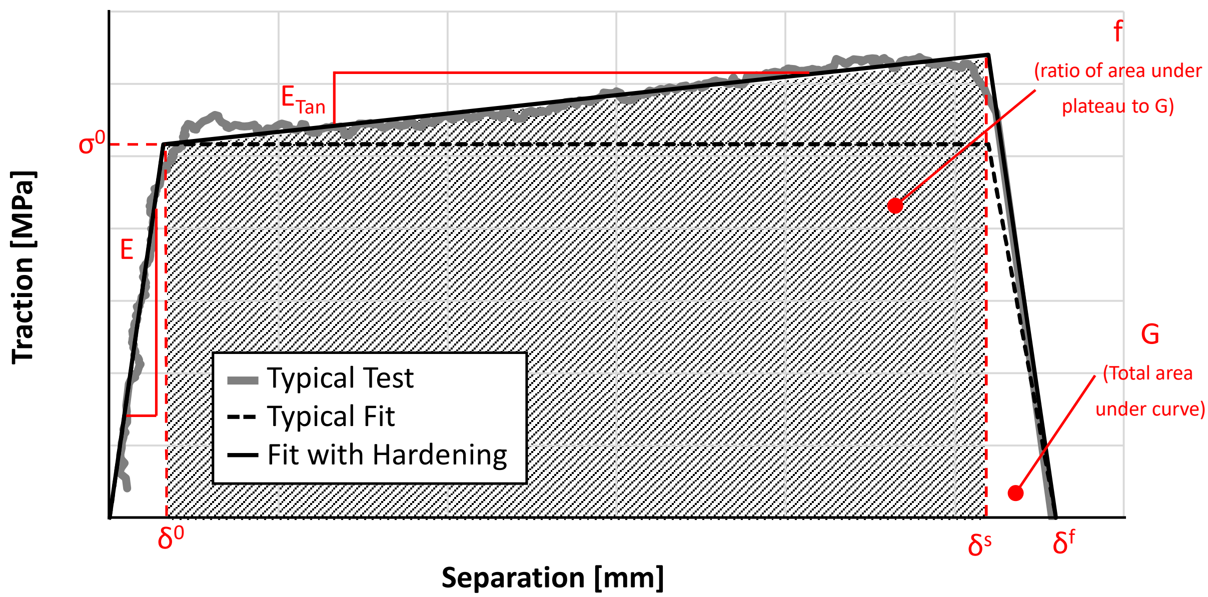

Figure 1: Trapezoidal traction-separation response highlighting parameter definition and separation measurements used in fit

The ratio of the Mode II separation (δ_{II}) to the Mode I separation (δ_I), mixity (β), is used to define the resultant mixed mode separation-to-plateau and separation-to-softening (Table 1). Separation-to-failure (δ^f), which is the separation at which the element no longer supports load and is removed from the simulation, is generally defined using relationships based on critical energy release rates (G_{IC}, G_{IIC}), such as the failure criterion suggested by Benzeggagh and Kenane [20] or power law relationships such as that proposed by Camanho & Dávila [16]. To define failure criteria based on critical energy release rates, the initial stiffness in Mode I and Mode II loading (E_I and E_{II}, respectively) are also required. δ^0, δ^s, and δ^f are recalculated at each timestep in the finite element simulation as the ratio between separation in the Mode I and Mode II directions evolves, although the other parameters are typically fixed throughout the simulation based on the material parameters defined in the model input. To account for potential non-linearities in the mixed mode failure response, an experimentally measured mixity failure parameter (η) has been proposed to control the mixed mode separation to failure [4,16], although the ability to fit the model traction-separation response to the experimental data can be somewhat limited.

Table 1: Summary of trapezoidal cohesive zone model mixity treatments

Separation Measure	**Resultant separation expressed using mode mixity ($\beta = \delta_{II/}\,\delta_I$)**
Separation-to-Plateau [16]	$\delta^0 = \delta_I{}^0 \cdot \delta_{II}{}^0 \sqrt{\dfrac{1+\beta^2}{\left(\delta_{II}{}^0\right)^2 + \left(\beta\delta_I{}^0\right)^2}}$
Separation-to-Softening [16]	$\delta^s = \delta_I{}^s \cdot \delta_{II}{}^s \sqrt{\dfrac{1+\beta^2}{(\delta_{II}{}^s)^2 + (\beta \cdot \delta_I{}^s)^2}}$
Separation-to-Failure (Power law [16])	$\delta^f = \dfrac{2(1+\beta^2)}{\delta_0}\left[\left(\dfrac{E_I}{G_{IC}}\right)^\eta + \left(\dfrac{\beta^2 \cdot E_{II}}{G_{IIC}}\right)^\eta\right]^{-1/\eta} + \delta_0 - \delta_s$
Separation-to-Failure (Benzeggagh-Kenane [20])	$\delta^f = \dfrac{2\left[G_{IC} + (G_{IIC} - G_{IC})\left(\dfrac{\beta^2 \cdot E_{II}}{E_I + \beta^2 \cdot E_{II}}\right)^\eta\right]}{\delta_0\left(\dfrac{E_I + \beta^2 \cdot E_{II}}{1+\beta^2}\right)} + \delta_0 - \delta_s$

In general, the initial Mode I and Mode II stiffness values are not equal, so care must be taken when assessing the mixed mode measurement because the resultant traction and resultant separation vectors will not align [18]. Due to the Mode I and Mode II plateau tractions being calculated based on the multiplication of the respective initial stiffness and separation-to-plateau for each mode, there is also little flexibility in representing the value of the resultant plateau traction.

Factors such as the thickness of the bond line [21-23], the rate of loading [17,24], previous cyclic loading history [25], humidity [26], and temperature of the adhesive joint [27,28] can affect the response of the adhesive. These effects are particularly well documented for the critical energy release rate and plateau (or peak) traction [4]. For the bond line thicknesses considered in the study presented in the current work (0.18 mm to 0.6 mm), increasing bond line thickness tends to reduce the peak traction [29] and increase the critical energy release rate for toughened epoxy adhesives [30]. CZM implementations generally only consider a single bond line thickness, so different sets of material parameters are required for each bond line thickness used in a finite element model.

Watson *et al.* [18,31] developed test methodologies to measure the complete traction-separation response of structural adhesives. In that study, the authors used these new test methodologies to measure the complete traction-separation response for Mode I, Mode II and a pair of mixed modes of loading (45° and 75°) for three bond line thicknesses (0.18 mm, 0.3 mm and 0.64 mm). The Mode I response was measured using the Rigid Double Cantilever Beam (RDCB) test specimen in which the force-displacement response was converted into traction-separation by using adherends with a large second-moment of area in the bending direction. This design allows for the assumption that the adherend is effectively rigid, concentrating the deformation in the adhesive bond line [31]. A similar approach was taken to design specimens in which the bond line could be loaded at 45°, 75°, and 90° with large bending resistance in the direction of loading. By using optical methods to measure separation across the bond line and dividing the measured force by the original bond line area measured prior to testing, the Mode II and mixed mode traction-separation response could be extracted. The measured parameters (G_C, E, f, and σ_0, for Mode I and Mode II) were fit to a trilinear CZM using a power law separation-to-failure with η = 1 (see line 3 in Table 1) [32] implemented using CZM elements in a commercial finite element solver (LS-DYNA). The prediction of the traction-separation response of the CZM under mixed mode loading was found to be poor [18] with the CZM overpredicting the mixed mode plateau traction. Additionally, the separation-to-softening was generally underpredicted for the mixed mode cases, leading to a shorter plateau and an extended softening region than was observed in the experiments. Additionally, three separate sets of material parameters were required to define each of the three bond line thicknesses investigated.

In the current study, an enhanced CZM was developed to address shortcomings of CZM implementations to accurately capture the traction-separation response across a range of mode mixity and bond line thickness combinations for toughened adhesives identified by Watson *et al*. [18]. The new approach utilized an evolving set of CZM parameters (E, E_{Tan}, σ_0, G and f) based on the mode mixity of each element throughout the simulation and the bond line thickness at the start of the simulation. The proposed model was then verified by modeling experimental characterization tests of Mode I, Mode II and mixed mode loading. The EMC was compared to a CZM implemented using an approach to mixity outlined in Table 1 (with a power law separation-to-failure definition using $\eta = 1$) [32], termed the 'Baseline' model, in order to demonstrate the ability of the new model to better represent the measured material response.

2 Model Methodology

2.1 Enhanced Mixed Mode Cohesive Zone Model Methodology

A new CZM, termed the 'Enhanced Mixed Mode Cohesive Zone' (EMC) Model, was developed to predict the traction-separation response of adhesive joints, improving on aspects of the mixed-mode response identified by Watson *et al*. [31] and adding effects of bond line thickness into a new CZM implementation. While the CZM approach was developed for zero or near-zero thickness bond lines with thicker bond lines potentially being modeled using a series of solid and CZM elements, the ultimate goal for this work is to utilize the EMC in large-scale finite element models for automobile crashworthiness applications. Solid element formulations of the adhesive were not investigated due to the small timestep sizes that would be associated with solid elements having thicknesses on the order of the bond line thicknesses used in the present study. The measured traction-separation responses presented by Watson *et al*. [31] were used to verify the EMC and compare it to a baseline CZM. The philosophy guiding the EMC was to use the resultant traction (σ)-resultant separation (δ) (*i.e.* the vector summation of Mode I and Mode II traction and separation) along the direction of mixed separation, rather than treat the two responses independently, as is typically the case, in order to predict the mixed-mode traction and failure of adhesive joints under complex loading. Furthermore, the EMC approach alleviates the misalignment of the traction and separation vectors under mixed mode loading due to unequal Mode I and Mode II stiffnesses noted by Watson *et al*. [31].

In the EMC model, a series of functions of mixity,

$$\Theta = \frac{2}{\pi} \cdot atan\left(\frac{\delta_{II}}{\langle \delta_I \rangle}\right), \tag{1}$$

and initial thickness of the element (t) are used to define the parameters necessary to construct the traction-separation response (E, σ_0, G, f, E_{Tan}, see Figure 1). The intention of this using this definition of mixity rather than the more traditional definition ($\beta = \delta_{II}/\delta_I$), was to define mixity between zero in Mode I and 1.0 in Mode II, rather than zero to infinity. The finite bounds of the new mixity definition were required for the parameter fitting described below. Furthermore, the new definition avoids values that approach infinity when the Mode I separation is very small, which could lead to round-off errors. Throughout the simulations, the mixity is calculated for each timestep, while the thickness is kept constant (equal to the initial thickness of the element). The separation-to-plateau (δ^0) of the resultant traction-resultant separation response for a given combination of Θ and t is defined in the typical manner found in the literature [16];

$$\delta^0 = \frac{\sigma_0}{E}. \tag{2}$$

The introduction of the hardening parameter E_{Tan} (see Figure 1), leads to definitions of the traction at the end of the plateau (σ_s) of

$$\sigma_s = \sigma_0 + E_{Tan} \cdot \left(\delta^s - \delta^0\right) \tag{3}$$

And the area under the plateau of

$$f \cdot G_C = \frac{1}{2} \cdot (\sigma_0 + \sigma_s) \cdot \left(\delta^s - \delta^0\right). \tag{4}$$

The total area under the traction-separation response (G_c) can be defined as

$$G_C = \frac{1}{2} \cdot \sigma_0 \cdot \delta^0 + f \cdot G_C + \frac{1}{2} \cdot \sigma_s \cdot \left(\delta^f - \delta^s\right). \tag{5}$$

Equation (3), Equation (4) and Equation (5) represent three equations with three unknown values (δ^s, δ^f, and σ_s). By rearraigning and substituting these equations the separation-to-softening (δ^s) can be shown to be as

$$\delta^s = \frac{\frac{2\sigma_0 E_{Tan}}{E} - 2\sigma_0 + \sqrt{\left(2\sigma_0 - \frac{2\sigma_0 E_{Tan}}{E}\right)^2 - \frac{2{E_{Tan}}^2{\sigma_0}^2}{E^2} - \frac{8E_{Tan}{\sigma_0}^2}{E} - 8fGE_{Tan}}}{2E_{Tan}}, \tag{6}$$

and the separation-to-failure (δ^f) is defined as

$$\delta^f = \frac{2 \cdot G(1-f) - \frac{{\sigma_0}^2}{E}}{\sigma_0 + E_{Tan}(\delta^s - \delta^0)} + \delta^s. \tag{7}$$

For a complete definition of the EMC, as with all CZM implementations, damage must be considered. For ease of calculation, two separate parameters are introduced. The first damage parameter (D) governs the traction response during unloading and reloading of the CZM element [33];

$$D = max\left(1-\frac{\delta^0}{\delta}, 1-\frac{\delta^0}{\delta}\cdot\frac{\delta^f-\delta}{\delta^f-\delta^s}, D_{previous}, 0\right). \tag{8}$$

The *previous* subscript denotes the damage from the previous time step. In this definition, D begins to accumulate once the resultant separation exceeds the δ^0 value. This formulation ensures the traction response returns to zero when the element is unloaded at any point during the loading history, without a permanent plastic set. This behaviour follows the conclusions found by Biel & Stigh [34], who measured the effect of damage on bonded DCB specimens and concluded that, while some residual displacement may be present, the unloading response is best described by a relationship that returns to zero separation when fully unloaded, with no permanent deformation.

A softening parameter (S),

$$S = max\left(1-\frac{\delta^f-\delta}{\delta^f-\delta^s}, S_{previous}, 0\right), \tag{9}$$

is added to govern the traction response between δ^S and δ^f. Conceptually, this parameter can be thought of as a damage parameter related to failure (rather than D, which is used to govern the unloading response). Unlike D, the softening parameter (S) only begins to increase after the resultant displacement exceeds δ^S. When S reaches unity, the element is unable to support further load and is eroded (removed) from the model.

The manner in which traction is calculated is dependent on the level of separation in the previous time step, namely,

$$\sigma = \begin{cases} (\delta-\delta_{t-1})\cdot\left((1-D)\cdot\left(E-E_{Tan}\cdot(1-S)\right)+E_{Tan}\cdot(1-S)\right)+\sigma_{previous} & \begin{matrix} if\ \delta-\delta_{previous}<0 \\ or\ \sigma_{previous}<\left(\sigma_0+E_{Tan}\cdot(\delta-\delta^0)\right)(1-S). \end{matrix} \\ \left(\sigma_0+E_{Tan}\cdot(\delta-\delta^0)\right)(1-S) & otherwise \end{cases} \tag{10}$$

The first step in calculating traction from a set of separation values for a given timestep, is to calculate the incremental displacement between the current resultant separation (δ) and the resultant separation from the previous time step ($\delta_{previous}$). If the change in displacement is less than zero (unloading) or the resultant traction from the previous timestep ($\sigma_{previous}$) is less than the plateau traction (which can occur during initial loading, reloading after unloading and the portion of the response between δ^S and δ^f), an incremental portion of traction is added to $\sigma_{previous}$ (as described in the first condition of Equation (10)). This traction increment accounts for any damage and softening, which may have occurred since the start of the simulation. Otherwise, the traction is set to the plateau traction for a given resultant separation along the direction of mixity (as described in the final condition of Equation (10)).

After calculating the resultant traction, the traction in Mode I and the two Mode II directions is required by the finite element solver. The resultant traction can be apportioned in the Mode II directions by

$$\sigma_{II,i} = \frac{\sigma \cdot tan\left(\frac{\pi}{2} \cdot \Theta\right)}{\sqrt{1 + tan^2\left(\frac{\pi}{2} \cdot \Theta\right)}} \cdot \frac{\delta_{II,i}}{\delta_{II}}, \ i = x, y. \tag{11}$$

The Mode I traction is somewhat more complicated due to the elastic, undamaging compression traction response typically assumed in CZM implementations. To account for this asymmetry, the Mode I traction is calculated as

$$\sigma_I = \begin{cases} \frac{\sigma}{\sqrt{1 + tan^2\left(\frac{\pi}{2} \cdot \Theta\right)}} & if\ \delta_I \geq 0 \\ E_{0^\circ} \cdot \delta_I & if\ \delta_I < 0 \end{cases}, \tag{12}$$

where E_{0° is the initial Mode I (0°) stiffness calculated for the bond line thickness originally defined for the given CZM element.

2.2 EMC Model Parameter Fitting from Characterization Data

To define the EMC model, the Mode II and mixed mode test presented in Watson *et al*. [18] were refit to include hardening, using a least squares approach for each test. Five test repeats of each mode of loading and bond line thickness combination were considered in the parameter fitting and model comparison. The Mode I test response did not exhibit appreciable hardening behaviour, although to avoid an infinite value for separation-to-softening (Equation (6)), an E_{Tan} value of $1\text{x}10^{-9}$ GPa/mm was used in all Mode I cases. Other adhesives may exhibit more hardening (or softening) in Mode I loading, which would be admissible using the current modelling approach. The average value of the CZM parameters were calculated for each combination of bond line thickness and mode mixity by curve fitting the individual tests presented in Watson *et al*. [18] to Equation (2) through Equation (7) using a non-linear least squares fitting approach. The mean values for each condition were then calculated to develop 'average' traction-separation responses (Table 2). Using these average parameters, a trapezoidal traction-separation response could be defined for each loading mode and bond line thickness combination tested.

Table 2: Summary of experimental test results for parameter fitting

Loading Angle [°]	Mixity (Θ)	Average bond line Thickness (t) [mm]	Initial Stiffness (E) [GPa/m]	Plateau Traction (σ_0) [MPa]	Critical Energy Release Rate (G) [kN/m]	Area Ratio (f)	Tangent Stiffness (E_{Tan}) [GPa/mm]
0	0	0.19 ± 0.04	2589	53.38	1.57	0.51	$1\text{x}10^{-9}$
		0.31 ± 0.01	1762	51.24	2.13	0.49	$1\text{x}10^{-9}$
		0.63 ± 0.01	1259	48.72	2.22	0.36	$1\text{x}10^{-9}$
45	0.5	0.23 ± 0.05	2417	30.60	2.05	0.87	0.04
		0.33 ± 0.05	2099	31.47	2.43	0.87	7.78
		0.60 ± 0.04	1242	28.42	3.60	0.79	0.03
75	0.833	0.24 ± 0.03	2542	26.36	5.01	0.95	10.46
		0.32 ± 0.03	1647	25.22	6.71	0.92	12.38
		0.61 ± 0.03	777	23.95	10.56	0.91	3.90
90	1	0.21 ± 0.04	2693	26.65	5.05	0.96	42.61
		0.38 ± 0.04	1903	26.71	7.29	0.97	16.28
		0.59 ± 0.04	772	23.65	13.76	0.95	8.33

For the baseline models, the CZM parameters presented in Watson *et al*. [18] were used directly to define the Mode I and Mode II behaviour using a trapezoidal traction-separation law. The mixed mode response was governed using a power law fit (see Table 1) with $\eta = 1$.

To identify functions of Θ and t for each parameter, surface fitting software (TableCurve 3D, Systat Software; San Jose, CA, USA) was used to determine the best fitting rational function. The rational function form that produced the highest r^2 value for each parameter was used, disregarding the functions that produced singularities over the domain of interest. Furthermore, the surface generated from each fit was examined to ensure the relationship matched observed trends in the experiments by Watson *et al.* [18]. For example, in the experiments, the plateau traction monotonically increased with thickness and monotonically decreased with Θ. The phenomenological relationships used to describe each parameter should be considered valid only for the range of bond line thicknesses tested (0.18 mm to 0.64 mm). The functions used to generate each parameter were as follows:

$$E(\Theta,t) = E_a + E_b\Theta + E_c t + E_d\Theta t + E_e\Theta^2 + E_f t^2 + E_g\Theta^2 t + E_h\Theta t^2 \tag{13}$$

$$\sigma_0(\Theta,t) = \sigma_{0,a} + \sigma_{0,b}\Theta + \sigma_{0,c}t + \sigma_{0,d}\Theta t + \sigma_{0,e}\Theta^2 + \sigma_{0,f}t^2 + \sigma_{0,g}\Theta^2 t + \sigma_{0,h}\Theta t^2 \tag{14}$$

$$G(t,\Theta) = \frac{G_a + G_b\Theta + G_c t + G_d t^2}{1 + G_e\Theta + G_f\Theta^2 + G_g\Theta^3 + G_h t} \tag{15}$$

$$f(\Theta,t) = f_a + f_b\Theta + f_c t + f_d\Theta t + f_e\Theta^2 + f_f t^2 + f_g\Theta^2 t + f_h\Theta t^2 \tag{16}$$

$$\begin{aligned} E_{Tan}(\Theta,t) = {} & E_{Tan,a} + E_{Tan,b}\Theta + E_{Tan,c}t + E_{Tan,d}\Theta t + E_{Tan,e}\Theta^2 + E_{Tan,f}t^2 \\ & + E_{Tan,g}\Theta^2 t + E_{Tan,h}\Theta t^2 \end{aligned} \tag{17}$$

While Equation (13) to Equation (17) were selected due to their ability to phenomenologically describe the test response well, further refinement to the function selection may simplify the input necessary to the model. Furthermore, additional factors such as loading rate, temperature, or environmental degradation due to surface contamination, or under or overcuring, could be included in these functions to account for such effects in future work, provided that test data is available.

2.3 Description of the Characterization Test Verification Models

In order to verify the EMC, simulations of the characterization tests were performed. The EMC model was implemented in a commercial explicit finite element solver (LS-DYNA Version 9.2.0 (build 119543), 64-bit, MPP, double precision) using a user-defined cohesive zone model subroutine.

The models of each characterization test (Figure 2) used 0.5 mm fully integrated (LS-DYNA, element type 2) hexahedral elements to model the adherends and loading pins in three dimensions (*i.e.* not using plane strain or plane stress elements). The total thickness of each specimen was modeled to match thickness from each test, 6.35 mm for the RDCB specimens and 3.18 mm for the shear and mixed mode specimens. An elastic material property was applied to the adherends (ρ = 7800 kg/m^3, E = 207 GPa and ν = 0.3). The loading pins were defined as rigid with one pin fixed in all directions and a prescribed velocity of 1.0 mm/s being applied to the other for 1 second of simulation time. The force required to maintain the separation was output to track loading force. For the RDCB models, displacement was measured by tracking the displacement of the loading pin, while in the remaining characterization models the displacement was tracked by measuring the relative displacement of the node on either side of the center of the bond line on the surface element, as was reported in the experiments.

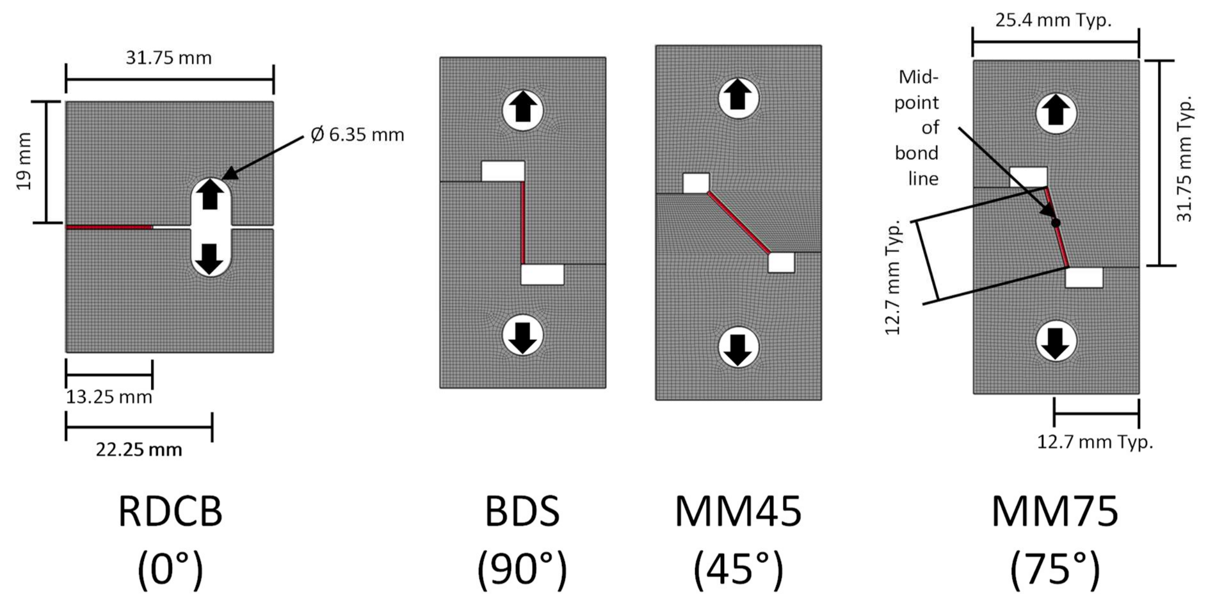

Figure 2: Finite element mesh of specimen geometry [18] used to extract the traction separation response under Mode I (RDCB), Mode II (BDS), and mixed mode (MM45 and MM75) loading

3 Results and Discussion

3.1 Fitting of the EMC Model to Experimental Characterization Test Data

When fitting the experimental data (Table 2) for each parameter (Table 3), the resulting surface plots provided a good fit to the measured data (Figure 3), with an average r^2 value of 0.97. Parameter fitting was performed using average test responses for each loading mode/bond line thickness combination. Using the individual test responses was found to only change the resulting predicted traction-separation responses by a maximum of 2% for the separation responses of interest (δ^0, δ^S, δ^f). The difference between the traction predicted using parameters fit from average or individual tests was an order of magnitude lower (0.2%) than the separation responses, due to lower variability in the force measurement in the characterization testing.

Table 3: Summary of EMC parameter function fitting (see Equation (13) to Equation (17))

Initial Stiffness (*E*) Parameters		**Plateau Traction (σ_0) Parameters**		**Critical Energy Release Rate (*G*) Parameters**		**Area Ratio (*f*) Parameters**		**Tangent Stiffness (E_{Tan}) Parameters**	
E_a [GPa m^{-1}]	4.46E+3	$\sigma_{0,a}$ [MPa]	5.68E+1	G_a [kN m^{-1}]	7.60E-1	f_a [MPa]	4.90E-1	$E_{Tan,a}$ [GPa m^{-1}]	-1.40E+1
E_b [GPa m^{-1}]	-1.29E+3	$\sigma_{0,b}$ [MPa]	-7.05E+1	G_b [kN m^{-1}]	1.30E-1	f_b [MPa]	1.02E+0	$E_{Tan,b}$ [GPa m^{-1}]	-9.62E+0
E_c [GPa m^{-2}]	-1.20E+1	$\sigma_{0,c}$ [MPa m^{-1}]	-2.13E-2	G_c [kN m^{-2}]	4.85E-3	f_c [MPa m^{-1}]	2.10E-4	$E_{Tan,c}$ [GPa m^{-2}]	8.67E-2
E_d [GPa m^{-2}]	8.94E+0	$\sigma_{0,d}$ [MPa m^{-1}]	5.24E-2	G_d [kN m^{-3}]	-5.74E-6	f_d [MPa m^{-1}]	-2.30E-4	$E_{Tan,d}$ [GPa m^{-2}]	-1.59E-1
E_e [GPa m^{-1}]	6.60E+2	$\sigma_{0,e}$ [MPa]	3.80E+1	G_e [kN m^{-1}]	1.11E+0	f_e [MPa]	-5.70E-1	$E_{Tan,e}$ [GPa m^{-1}]	9.99E+1
E_f [GPa m^{-3}]	1.10E-2	$\sigma_{0,f}$ [MPa m^{-2}]	1.31E-5	G_f [kN m^{-1}]	-4.13E+0	f_f [MPa m^{-2}]	-6.50E-7	$E_{Tan,f}$ [GPa m^{-3}]	-1.04E-4
E_g [GPa m^{-2}]	-2.74E+0	$\sigma_{0,g}$ [MPa m^{-1}]	-1.40E-2	G_g [kN m^{-1}]	2.46E+0	f_g [MPa m^{-1}]	1.20E-4	$E_{Tan,g}$ [GPa m^{-2}]	-1.51E-1
E_h [GPa m^{-3}]	-1.01E-2	$\sigma_{0,h}$ [MPa m^{-2}]	-4.35E-5	G_h [kN^{-1}]	-5.30E+2	f_h [MPa m^{-2}]	5.10E-7	$E_{Tan,h}$ [GPa m^{-3}]	2.84E-4

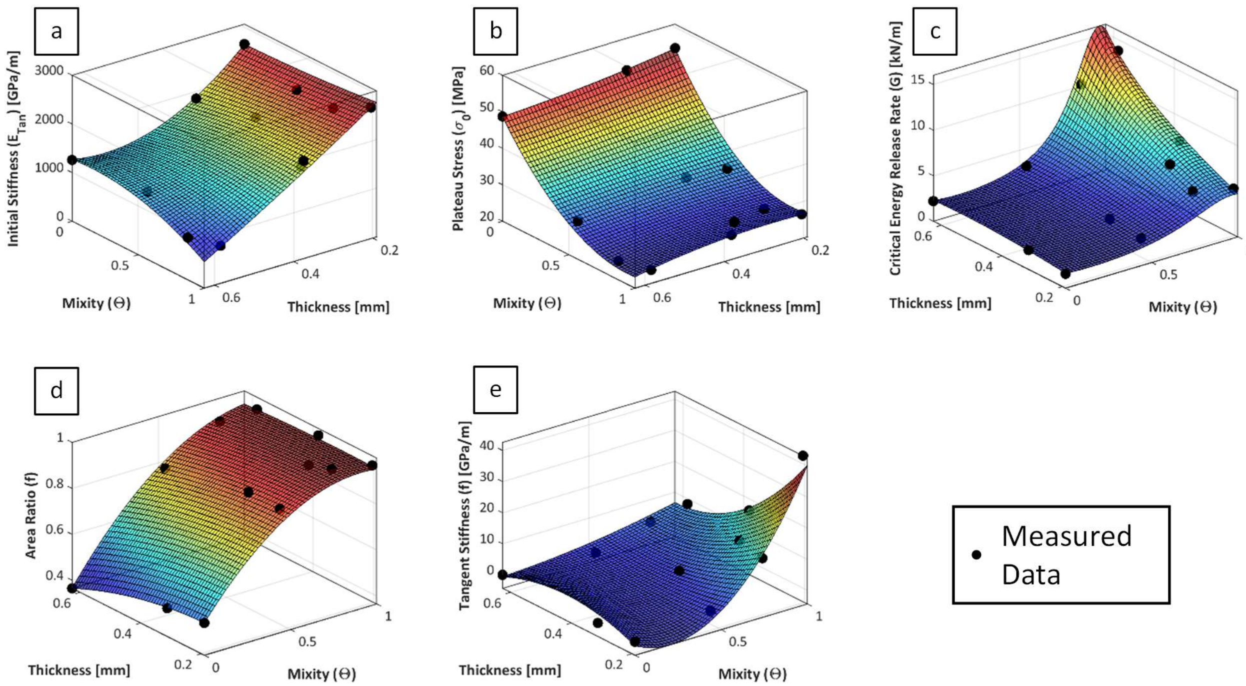

Figure 3: EMC parameter fitting as a function of mixity (*Θ*) and bond line thickness (*t*) for initial stiffness (a, r^2 = 0.95), plateau traction (b, r^2 = 0.99), critical energy release rate (c, r^2 = 0.99), area ratio (d, r^2 = 0.99) and tangent stiffness (e, r^2 =0.90) (see Figure 1)

3.2 Verification of the EMC Model Through Comparison to the Experimental Data

The verification models of the RDCB tests using the EMC approach provided a good fit to both the output force-displacement response (Figure 4a, b, c) and calculated traction-separation response (Figure 4d, e, f). The maximum force predicted by the EMC models was within 2.5% of the experimental average. After converting the force-displacement response to traction-separation, the average of the separation responses (δ^0, δ^S, δ^f) of the models was within 8% of the experimental average, while the average plateau traction was within 2%. The baseline CZMs also demonstrated good agreement with the test response. Both the EMC and baseline models of the 0.18 mm nominal bond line thickness did have some difficulty capturing the abrupt drop in the force-displacement response that was observed during testing (Figure 4a). This lack of fit was partly due to the underlying assumptions of the CZM approach, which assumes an area of damaged material is present in front of the crack tip [35, 36], which was not the case in the brittle fracture present in these tests. Despite the limitation of the CZM approach to capture brittle fracture, the traction-separation response generated from the models of the RDCB test was able to capture the test response reasonably well. Some discrepancy was apparent between the experimental (input) average traction-separation responses and that generated by the models, due to the compliance of the elastic adherends rather than the perfectly-rigid adherend assumption embedded in the analysis technique [18, 31]. Additionally, the fixed 21 point running average used smooth the force-displacement response to aid in the numerical differentiation required for conversion of the force-displacement to traction-separation [31] may have introduced some differences between the model and expected response due to the higher sampling rate of model compared to the tests.

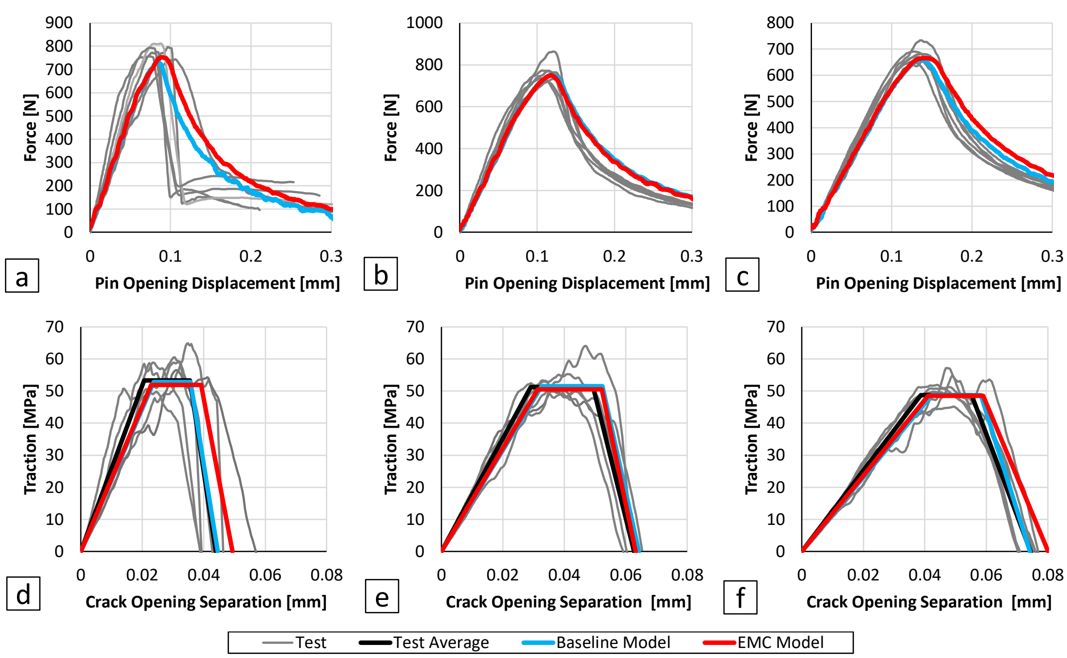

Figure 4: Comparison of RDCB CZMs to experimental [18] force-displacement response and corresponding output of traction-separation for nominal bond line thicknesses of 0.18 mm (a,d), 0.3 mm (b,e), and 0.64 mm (c,f)

The models using the EMC approach were in good agreement with the measured response (Figure 5) with an average error of 5% and 1% for the separation values (δ^0, δ^S, δ^f) and average traction values, respectively. The baseline model also provided the expected response, although without capturing the hardening behaviour of the test data.

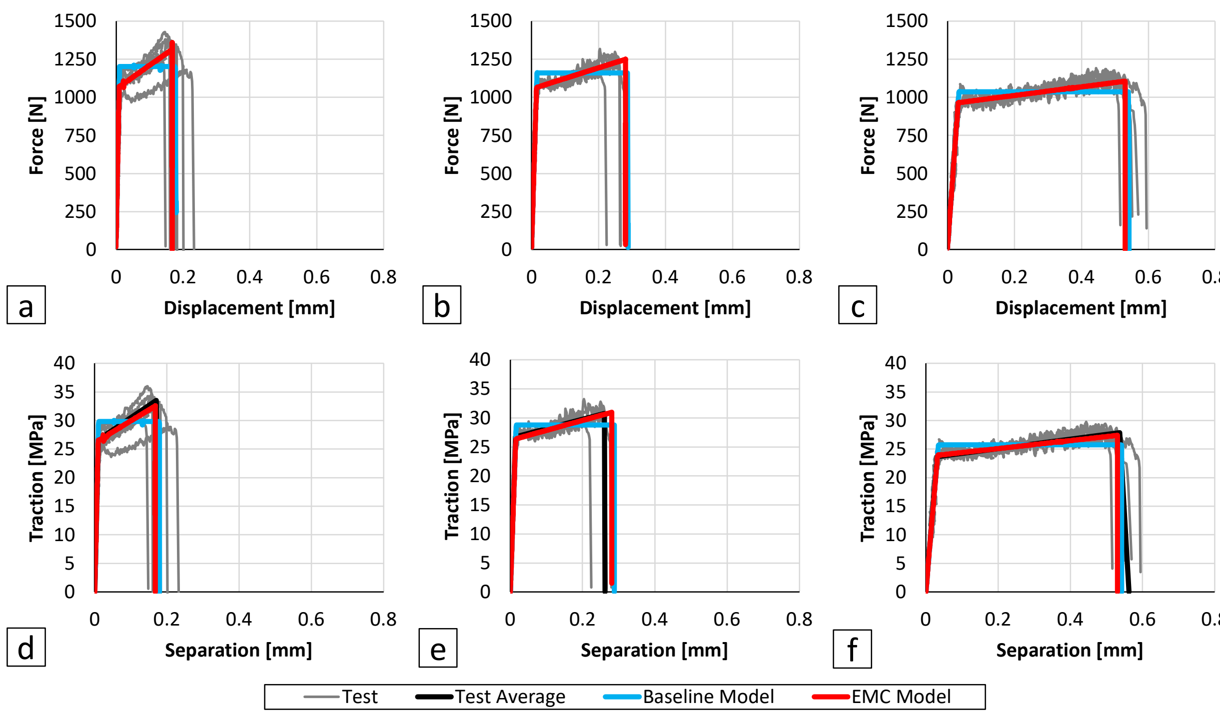

Figure 5: Comparison of BDS CZMs to experimental [18] force-displacement response and corresponding output of traction-separation for nominal bond line thicknesses of 0.18 mm (a,d), 0.3 mm (b,e), and 0.64 mm (c,f)

The 45° mixed mode EMC models generally reproduced the experimental response well, with the δ^0, δ^S, and δ^f values predicted within an average of 2% and average traction within 7%, compared to 14% and 24%, respectively, for the baseline model (Figure 6). Despite the EMC models reproducing the test response well, some deviation was apparent in the softening portion, particularly for the thickest bond line (Figure 6c). For this bond line thickness, the mixity prior to failure near the end of the bond line ranged from 0.48 to 0.53, compared to 0.5 in the ideal scenario.

This slight change in mixity led to differences in the traction-separation responses for individual elements at the ends of the bond line. These deviations and the small difference between the δ^S and δ^f values, led to earlier softening of the elements at the end of the bond line compared to elements away from the ends. A rebalancing of load across the bond line was then necessary, which led to failure of the whole bond area earlier than would otherwise be expected. The minor variation in mixity leading to abrupt failure occurred in the softening portion of the baseline model response for all three bond line thicknesses, compared to the plateau portion of the response for the EMC models. The baseline model also tended to exhibit a higher plateau traction, a lower separation between the start and end of the plateau and a greater separation between softening onset and failure.

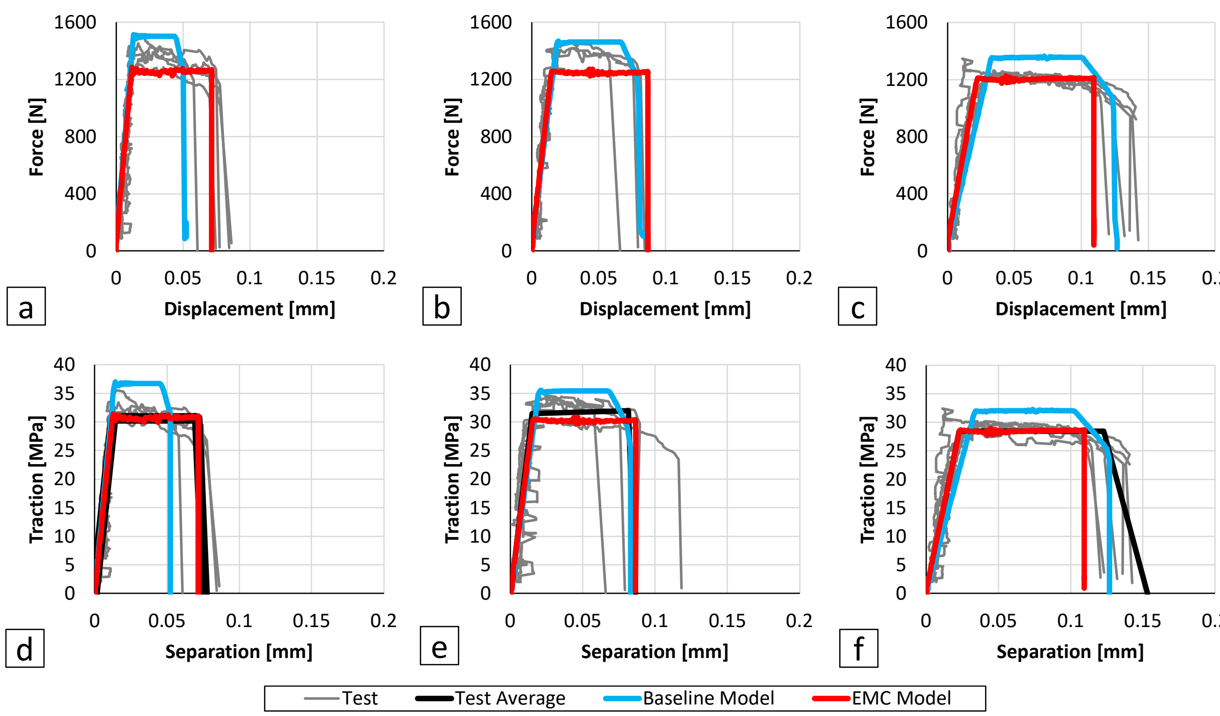

Figure 6: Comparison of 45° MM CZMs to experimental [18] force-displacement response and corresponding output of traction-separation for nominal bond line thicknesses of 0.18 mm (a,d), 0.3 mm (b,e), and 0.64 mm (c,e)

As with the 45° mixed mode models, the 75° mixed mode ECM model was substantially better at capturing the test response than the baseline models (Figure 7). Of particular note, the hardening aspect of the test response was more pronounced in the 75° mixed mode compared to 45°, which was captured by the rising plateau of the EMC models. Furthermore, the test and EMC models exhibited very little softening, failing abruptly, unlike the baseline models that exhibited much more pronounced softening behavior. Both the EMC and baseline models exhibited abrupt failure of elements, with the EMC models failing with essentially no progressive softening, as in the experiments. The baseline models, however, exhibited a large degree of softening prior to abrupt failure from relatively low traction values (less than 10 MPa) in all the bond line thicknesses.

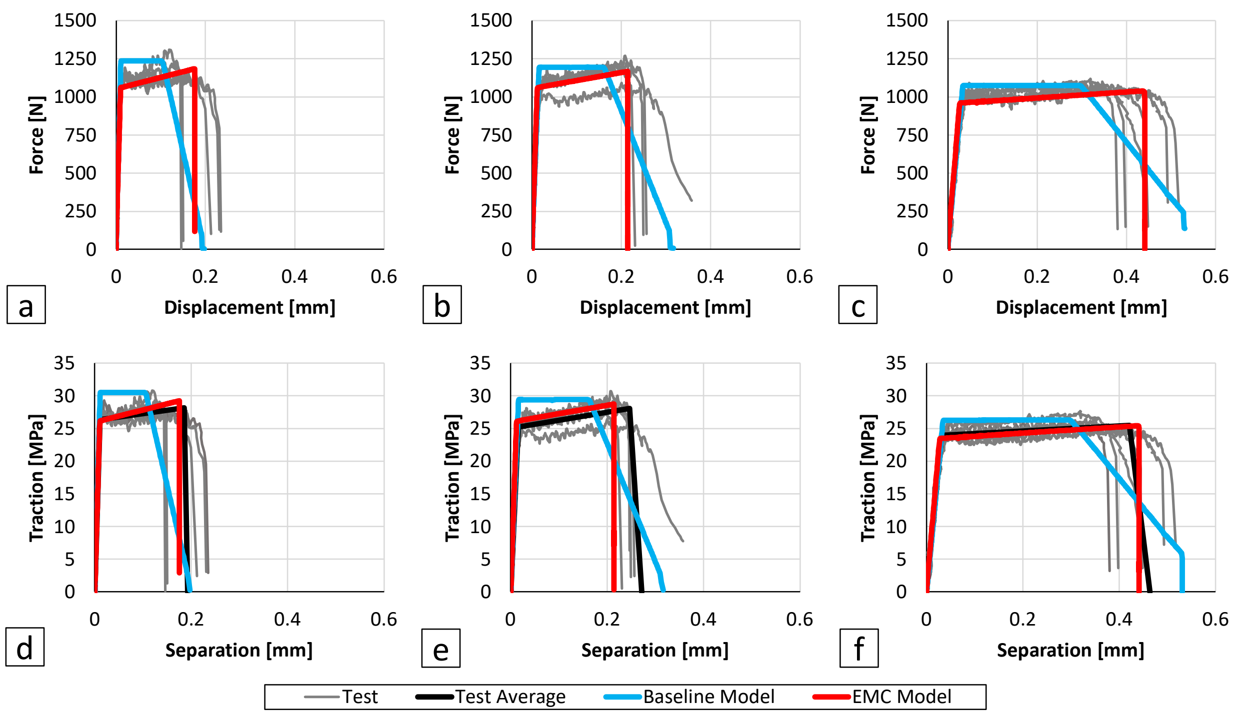

Figure 7: Comparison of 75° MM CZMs to force-displacement response and corresponding output of experimental [18] traction-separation for nominal bond line thicknesses of 0.18 mm (a ,d), 0.3 mm (b,e), and 0.64 mm (c,f)

The ability of the EMC model to accurately reproduce not only the pure Mode I and Mode II test response, but also the full traction-separation response for mixed modes of loading is an attractive feature of the EMC over traditional approaches, where control of the mixed mode response is somewhat limited. The average absolute difference between the model predictions and test average for δ^0, δ^s and δ^f were 11%, 8% and 12%, respectively, for the EMC models compared to 12%, 36% and 11% for the baseline CZM mixed mode models. Furthermore, the average absolute difference between the model and test traction at plateau and softening were 2% and 3%, respectively, for the EMC model, compared to 14% and 5% for the baseline CZM approach. Thus, it can be seen that the EMC approach addressed the over prediction of plateau traction and under prediction of plateau length under mixed mode loading identified by Watson *et al.* [18]. The reduction in error associated with the mixed modes of loading highlights the main advantage of the EMC approach over traditional treatment of mixed mode loading, despite providing similar levels of fit to the data for both approaches for pure Mode I and Mode II loading. The trade off for this improved fidelity in mixed mode response using the EMC approach is that testing is required to characterize the complete mixed mode traction-separation of a given adhesive [17, 18]. Furthermore, more data processing is required to derive a set of parameters to fully define the EMC model by first fitting E, E_{Tan}, σ_0, G and f to Mode I, Mode II and mixed mode test responses and then fitting these CZM parameters to Equation (13) through Equation (17) rather than only defining the Mode I and Mode II CZM parameters. However, a single set of parameters can be used to model a range of bond line thickness, potentially simplifying the input in large-scale models which use multiple bond line thicknesses.

The fit parameters used in the current study can only be used in a relatively narrow band of bond line thicknesses (between 0.15 mm and 0.7 mm) before the emergence of non-valid traction-separation responses, caused by the combination of parameters leading to δ^f values that are less than the corresponding δ^S. Care must be taken to avoid these unphysical responses, although ideally one would ensure that the characterization tests were undertaken within the range of bond line thicknesses of interest for the models for which the EMC would ultimately be used.

The current study focused on the effects of bond line thickness on the traction-separation response under various modes of loading. However, the EMC approach could be adapted to investigate other effects such as temperature during loading, loading rate, the degree of under/overcuring of the adhesive or other environmental exposure effects. Obviously to investigate these effects, further experimentation would need to be carried out and Equation (13) through Equation (17) would need to be updated to include these effects for each parameter. A more refined definition of the model may also be required for effects that evolve during the simulation, such as the treatment of loading rate effects by May *et al.* [4]. Future work with the EMC model will involve validating the model by investigating the predictive capabilities using a series of cross tension tests with varying loading angles [37] to assess the model for a range of loading modes in scenarios beyond the verification carried out in the current study. Furthermore, an investigation which exercises the ability of the new CZM to assess the response of structures with bond lines of varying thicknesses (as opposed to a series of constant bond line thicknesses) will be carried out.

4 Conclusions

The Enhanced Mixed Mode CZM (EMC) incorporates greater control over the mixed mode response compared to CZMs that are used in current FE solvers (such as the baseline model), incorporating a hardening response rather than a plateau and can be implemented with a single set of parameters for a range of bond line thicknesses. By accounting for hardening of the adhesive joint under Mode II loading using the BDS specimen, the EMC approach eliminated the 13% average overprediction of traction at the start of the plateau and 10% underprediction of traction at the end of the plateau present in the baseline model. Furthermore, the EMC approach reduced the average difference between the model prediction and average test response for separation-to-plateau, softening and failure (8%) compared to a more traditional CZM approach (22%). The ECM approach can also readily be extended to account for factors altering the traction-separation response, such as temperatures, loading rate and environmental factors affecting curing.

Acknowledgements

The authors would like to express their thanks to Honda Development & Manufacturing of America, 3M Canada Company, ArcelorMittal, Ontario Centers of Excellence, the Ontario Advanced Manufacturing Consortium, Compute Canada and the Natural Sciences and Engineering Research Council of Canada (NSERC) for their support of this research.

Data Availability

The CZM developed in this study will be made available to the research community as a shared library that can be linked into the LS-DYNA finite element code. Please contact the corresponding author for information on accessing the CZM shared library.

Disclosure Statement

The authors report there are no competing interests to declare.

References

[1] Tserpes, K.; Barroso-Caro, A.; Carraro, P.A.; Beber, V.C.; Floros, I.; Gamon, W.; Kozłowski, M.; Santandrea, F.; Shahverdi, M.; Skejić, D.; Bedon, C.; Rajčić, V. A review on failure

theories and simulation models for adhesive joints. *The Journal of Adhesion*, **2022**, 98:12, 1855-1915, DOI: 10.1080/00218464.2021.1941903

[2] Matzenmiller, A.; Gerlach, S.; Fiolka, M. A critical analysis of interface constitutive models for the simulation of delamination in composites and failure of adhesive bonds. *Journal of Mechanics of Materials and Structures*. **2010**, 5(2), 185-211. DOI: 10.2140/jomms.2010.5.185

[3] Nossek, M.; Marzi, S. Cohesive zone modeling for adhesives. In *Predictive Modeling of Dynamic Processes*, 1st ed.; Hiermaier, S., Ed. Springer: Boston, MA., 2009; pp 89-105. DOI: 10.1007/978-1-4419-0727-1_5

[4] May, M.; Hesebeck, O.; Marzi, S.; Böhme, W.; Lienhard, J.; Kilchert, S.; Brede, M.; Hiermaier, S. Rate dependent behavior of crash-optimized adhesives–Experimental characterization, model development, and simulation. *Engineering Fracture Mechanics*. **2015**, 133, 112-137. DOI: 10.1016/j.engfracmech.2014.11.006

[5] Yan, C.C.; Ma, J.L.; Zhang, Y.X.; Wu, C.W.; Yang, P.; Wang, P.; Zhang, W.; Han, X. The fracture performance of adhesively bonded orthodontic brackets: an experimental-FE modelling study, *The Journal of Adhesion*, **2022**, 98:2, 180-206, DOI: 10.1080/00218464.2020.1826320

[6] Dantas, M.A.; Carbas, R.; Marques, E.A.S.; Parente, M.P.L.; Kushner, D.; da Silva, L.F.M. Numerical study of flexible tubular metal-polymer adhesive joints, *The Journal of Adhesion*, **2022**, 98:2, 131-153, DOI: 10.1080/00218464.2020.1822173

[7] Watson, B.; Nandwani, Y.; Worswick, M.J.; Cronin, D.S. Metallic multi-material adhesive joint testing and modeling for vehicle lightweighting. *International Journal of Adhesion and Adhesives*. **2019**, 95:102421,,DOI: 10.1016/j.ijadhadh.2019.102421.

[8] Akhavan-Safar, A.; Marques, E.A.S.; Carbas, R.J.C.; da Silva, L.F.M. Cohesive Zone Modelling-CZM. In *Cohesive Zone Modelling for Fatigue Life Analysis of Adhesive Joints*. Springer, Cham CH, **2022**, pp 19–43. DOI: 10.1007/978-3-030-93142-1_2

[9] Hillerborg, A.; Modéer, M.; Petersson, P. E. Analysis of crack formation and crack growth in concrete by means of fracture mechanics and finite elements. *Cement and Concrete Research*. **1976**, 6(6), 773-781. DOI: 10.1016/0008-8846(76)90007-7

[10] Alfano, G.; Crisfield, M.A. Finite element interface models for the delamination analysis of laminated composites: mechanical and computational issues. *International Journal for Numerical Methods in Engineering*. **2001**, 50, 1701–1736. DOI: 10.1002/nme.93

[11] Tvergaard, V.; Hutchinson, J. W. The relation between crack growth resistance and fracture process parameters in elastic-plastic solids. *Journal of the Mechanics and Physics of Solids*. **1992**, 40(6), 1377-1397. DOI: 10.1016/0022-5096(92)90020-3

[12] Yang, Q. D.; Thouless, M. D. Mixed-mode fracture analyses of plastically-deforming adhesive joints. *International Journal of Fracture*. **2001**, 110(2), 175-187. DOI: 10.1023/A:1010869706996

[13] Tvergaard, V.; Hutchinson, J. W. On the toughness of ductile adhesive joints. *Journal of the Mechanics and Physics of Solids*. **1996**, 44(5), 789-800. DOI: 10.1016/0022-5096(96)00011-7

[14] Feraren, P.; Jensen, H. M. Cohesive zone modelling of interface fracture near flaws in adhesive joints. *Engineering Fracture Mechanics*. **2004**, 71(15), 2125-2142. DOI: 10.1016/j.engfracmech.2003.12.003

[15] Trimiño, L. F.; Cronin, D. S. Evaluation of numerical methods to model structural adhesive response and failure in tension and shear loading. *Journal of Dynamic Behavior of Materials*. **2016**, 2(1), 122-137. DOI: 10.1007/s40870-016-0045-7

[16] Camanho, P. P.; Dávila, C. G. *Mixed-mode decohesion finite elements for the simulation of delamination in composite materials*; NASA/TM-2002-211737; NASA Langley Research Center: Hampton, VA, 2002. https://ntrs.nasa.gov/archive/nasa/casi.ntrs.nasa.gov/20020053651.pdf (accessed Oct 12, 2022).

[17] Lißner, M.; Alabort, E.; Cui, H.; Rito, R.; Blackman, B. R. K.; Petrinic, N. Experimental characterisation and numerical modelling of the influence of bondline thickness, loading rate, and deformation mode on the response of ductile adhesive interfaces. *Journal of the Mechanics and Physics of Solids*. **2019**, 130, 349-369. DOI: 10.1016/j.jmps.2019.06.011

[18] Watson, B.; Worswick, M. J.; Cronin, D. S. Quantification of Mixed Mode Loading and Bond Line Thickness on Adhesive Joint Strength Using Novel Test Specimen Geometry. *The International Journal of Adhesion and Adhesives*. **2020**, 102, 102682. DOI: 10.1016/j.ijadhadh.2020.102682

[19] Sun, Y.; Pugno, N.; Gong, B.; Ding, Q. A simplified hardening cohesive zone model for bondline thickness dependence on adhesive joints. *International Journal of Fracture*, **2015**, 194, 37–44, DOI: 10.1007/s10704-015-0036-z

[20] Benzeggagh, M. L.; Kenane, M. J. C. S. Measurement of mixed-mode delamination fracture toughness of unidirectional glass/epoxy composites with mixed-mode bending apparatus. *Composites Science and Technology*. **1996**, 56(4), 439-449. DOI: 10.1016/0266-3538(96)00005-X

[21] Lee, D. B.; Ikeda, T.; Miyazaki, N.; Choi, N. S. Effect of bond thickness on the fracture toughness of adhesive joints. *Journal of Engineering Materials and Technology*. **2004**, 126(1), 14-18. DOI: 10.1115/1.1631433

[22] da Silva, L. F.; Rodrigues, T. N. S. S.; Figueiredo, M. A. V.; De Moura, M. F. S. F.; Chousal, J. A. G. Effect of adhesive type and thickness on the lap shear strength. *The Journal of Adhesion*. **2006**, 82(11), 1091-1115. DOI: 10.1080/00218460600948511

[23] Boutar, Y.; Naïmi, S.; Mezlini, S.; da Silva, L. F.; Ali, M. B. S. Characterization of aluminium one-component polyurethane adhesive joints as a function of bond thickness for the automotive industry: Fracture analysis and behavior. *Engineering Fracture Mechanics*. **2017**, 177, 45-60. DOI: 10.1016/j.engfracmech.2017.03.044

[24] Sun, C.; Thouless, M. D.; Waas, A. M.; Schroeder, J. A.; Zavattieri, P. D. Rate effects for mixed-mode fracture of plastically-deforming, adhesively-bonded structures. *International Journal of Adhesion and Adhesives*. **2009**, 29(4), 434-443. DOI: 10.1016/j.ijadhadh.2008.09.003

[25] Akhavan-Safar, A.; Monteiro, J.; Carbas, R.; Marques, E.; Goyal, RK.; da Silva L. A modified degradation technique for fatigue life assessment of adhesive materials subjected to cyclic shear loads. *Proceedings of the Institution of Mechanical Engineers, Part C: Journal of Mechanical Engineering Science*, **2021**, 235(3), 550-559. DOI:10.1177/0954406220967684

[26] Chao, Y.; Ma, J.; Chen, Z.; Zhang, Y.; Yang, P.; Wang, S.; Wang, L.; Han, X.; Liu, Y.; Wu, C. Modelling prediction on the degradation in mode II fracture energy of structural adhesive subjected to hygrothermal ageing, *The Journal of Adhesion*, **2022**, 98:5, 553-575, DOI: 10.1080/00218464.2020.1859374

[27] Avendaño, R.; Carbas, R. J. C.; Marques, E. A. S.; da Silva, L. F. M.; Fernandes, A. A. Effect of temperature and strain rate on single lap joints with dissimilar lightweight adherends bonded with an acrylic adhesive. *Composite Structures*. **2016**, 152, 34-44. DOI: 10.1016/j.compstruct.2016.05.034

[28] Carlberger, T.; Biel, A.; Stigh, U. Influence of temperature and strain rate on cohesive properties of a structural epoxy adhesive. *International Journal of Fracture*. **2009**, 155(2), 155-166. DOI: 10.1007/s10704-009-9337-4

[29] Lißner, M.; Alabort, E.; Cui, H.; Pellegrino, A.; Petrinic, N. On the rate dependent behaviour of epoxy adhesive joints: Experimental characterisation and modelling of mode I failure. *Composite Structures*. **2018**, 189, 286-303. DOI: 10.1016/j.compstruct.2018.01.019

[30] Kinloch, A. J.; Shaw, S. J. The fracture resistance of a toughened epoxy adhesive. *The Journal of Adhesion*. **1981**, 12(1), 59-77. DOI: 10.1080/00218468108071189

[31] Watson, B.; Liao, C. H.; Worswick, M. J.; Cronin, D. S. Mode I traction-separation measured using rigid double cantilever beam applied to structural adhesive. *The Journal of Adhesion*. **2020**, 96(8), 717-737. DOI: 10.1080/00218464.2018.1502666

[32] Marzi, S.; Hesebeck, O.; Brede, M.; Kleiner, F. A rate-dependent cohesive zone model for adhesively bonded joints loaded in mode I. *Journal of Adhesion Science and Technology*. **2009**, 23(6), 881-898. DOI: 10.1163/156856109X411238

[33] de Moura, M. F. S. F.; Gonçalves, J. P. M.; Chousal, J. A. G.; Campilho, R. D. S. G. Cohesive and continuum mixed-mode damage models applied to the simulation of the mechanical behaviour of bonded joints. *International Journal of Adhesion and Adhesives*. **2008**, 28(8), 419-426. DOI: 10.1016/j.ijadhadh.2008.04.004

[34] Biel, A.; Stigh, U. Damage and plasticity in adhesive layer: an experimental study. *International Journal of Fracture*. **2010**, 165(1), 93-103. DOI: 10.1007/s10704-010-9508-3

[35] Barenblatt, G. I. The mathematical theory of equilibrium cracks in brittle fracture. *Advances in Applied Mechanics*. **1962**, 7(1), 55-129. DOI: 10.1016/S0065-2156(08)70121-2

[36] Ji, G.; Ouyang, Z.; Li, G.; Ibekwe, S.; Pang, S. S. Effects of adhesive thickness on global and local Mode-I interfacial fracture of bonded joints. *International Journal of Solids and Structures*. **2010**, 47(18-19), 2445-2458. DOI: 10.1016/j.ijsolstr.2010.05.006.

[37] Ibrahim, A. H.; Watson, B.; Jahed, H.; Rezaee, S.; Royer, C.; Cronin, D.S. Prediction of bonded asymmetric metallic cross-tension and single lap shear joints using finite element model with material-level adhesive properties and cohesive zone method. *International Journal of Adhesion and Adhesives*. **2022**, 120:103298. DOI : 10.1016/j.ijadhadh.2022.103298.